






## GROUND PENETRATING RADAR APPLIED TO ASPHALTIC PAVEMENTS - A STUDY IN A CONTROLLED SITE

Jéssica de Souza Moreira <sup>1\*</sup>, Maria Clara Lopes Paula <sup>1</sup>, Welitom Rodrigues Borges <sup>1</sup>,  
Antônio Lazaro Ferreira Santos <sup>2</sup>, and Eduardo Xavier Seimetz <sup>1</sup>

<sup>1</sup>Universidade de Brasília - UnB, Instituto de Geociências, Brasília, DF, Brazil

<sup>2</sup>Universidade Estadual de Goiás - UEG, Anápolis, GO, Brazil

\*Corresponding author email: [moreirageologia@gmail.com](mailto:moreirageologia@gmail.com)

**ABSTRACT.** The major challenges in road infrastructure studies are related to the evaluation of the road pavement quality in a practical, non-destructive, and low-cost way. Information about the thickness of the layers is fundamental to pavement repairing. In this study, the applicability of the ground penetrating radar (GPR) method in the delimitation of the pavement layer is tested at the Shallow Geophysical Test Site Applied to Engineering of Universidade Estadual de Goiás (UEG). The ground penetrating radar presents satisfactory results, identifying the top and bottom of the first five layers by the 270, 400, and 900 MHz antennas. The 2 GHz antenna was able to only delimit the top and bottom of the Hot Rolled Asphalt (HRA). The geomembrane with geotextile set and the concrete layer were not identified in the radargrams. The resolution of each antenna is 9.8 cm for 270 MHz; 6.0 cm for 400 MHz; 2.9 for 900 MHz; and 1.6 cm for 1600 MHz. Concerning layer thickness estimates, the antennas had an efficiency percentage of 83 % (270 and 1600 MHz), 83.29 % (400 MHz), and 84.40 % (900 MHz). Layer thickness estimates obtained by GPR antennas were compared with true thickness using a paired t-test ( $\alpha = 0.05$ ). No significant differences in layer thickness were observed for the GPR antennas versus the actual pavement thickness.

**Keywords:** GPR; geosynthetics; road investigation; shallow geophysical test site; non-destructive testing.

### INTRODUCTION

Test sites are important to understand forthcoming results in any geophysical survey, both geotechnical (Grandjean et al., 2000; Paniagua et al., 2004; Porsani et al., 2006; Borges, 2007; Orfanos & Apostolopoulos, 2012; Santos et al., 2019), and archeological (Porsani et al., 2006; Borges, 2007; Aragão et al., 2010), and forensic studies (Brasil, 2013; Cavalcanti, 2017; Canata et al., 2020). The previously known characteristics of buried targets, such as physical properties, geometry, and depth, collaborate in future interpretations of geophysical responses in different materials (Borges, 2007).

In France, researchers of the Central Laboratory of the Ponts and Chaussées (LCPC) carried out tests with different ground penetrating radar (GPR) techniques to discuss the performance of this method in civil engineering (Grandjean et al., 2000). Thereafter, other works with test sites applied to civil engineering were also performed in Spain (Paniagua et al., 2004) and Greece (Orfanos & Apostolopoulos, 2012).

In Brazil, the Shallow Geophysical Test Site of IAG-USP is one of the pioneers in geotechnical, archaeological, and environmental studies (Porsani et al., 2006; Borges, 2007). In 2018, researchers of the State University of Goiás (UEG) created the Shallow Geophysical Test Site Applied to Engineering of UEG (SCGRA-ENG) with the Goiás State Court of Auditors (TCE) and researchers from the University of Brasília (UnB) (Santos et al., 2019).

In this work, two pavements within the SCGRA-ENG will be investigated using the GPR method. The aim is to distinguish pavement layers using quantitative and qualitative results registered in radargrams generated by different center frequencies: 270 MHz, 400 MHz, 900 MHz, and 1600 MHz. Furthermore, analyses of each antenna radargram in each layer will be evaluated. Moreover, it will be discussed some parameters such as depth of investigation, sampling, and the resolution of each frequency in the stratigraphic context of the SCGRA-ENG.

## METHODOLOGY

This section comprises the following steps: (1) selection of the study object area, (2) acquisition of GPR data, and (3) data processing and interpretation. The Shallow Geophysical Test Site Applied to Engineering - UEG was created in the city of Anapólis, State of Goiás - Brazil (Figure 1).

This study selected line 1 of the SCGRA-ENG, containing two pavements, named line 1A and line 1B (Figure 2). For line 1A, the flexible pavement comprises layers of (first layer) a mixture of gap-graded aggregate, a filler aggregate, and a bitumen binder called Hot Rolled Asphalt (HRA). After that, a granular base, gravel No. 02, a rockfill, gravel No. 2, and a geomembrane with geotextile set in which the layers are inclined 2 degrees up on the south side. In line 1B, the flexible pavement consists of HRA, a granular base, gravel No. 2, a drainage banklet, gravel No. 2, and a geomembrane with geotextile set with horizontal layers.

### Data acquisition

The data acquisition was performed with different antenna frequencies: 270 MHz, 400 MHz, 900 MHz, and 1600 MHz. The survey was conducted using a GPR SIR4000 control unit from Geophysical Survey Systems Inc (GSSI). Line 1 was carried out in a common-offset mode for each antenna, covering two pavements per profile in the S/N direction. There, four profiles were performed along line 1. The profiles were acquired with trace intervals of 0.0033 m (for 270 and 1600 MHz) and 0.005 m (for 400 and 900 MHz), with 2048 samples for the 270 MHz antenna and 1024 samples for 400, 900, and 1600 MHz. The time window for 270 and 400 MHz was 60 ns, while for 900 MHz, the time window chosen was 53.33 ns. The time window for 1600 MHz was 46.77 ns. The acquisition parameters are shown in Table 1.

In addition to the visual interpretation of radar-grams, it was analyzed the envelope trace, which shows the intensity of the energy signal and allows visualizing changes in amplitudes that are significant. For amplitude analysis, it was collected acquisitions using the 1D point mode with antennas positioned in the center of each pavement. The same parameters used in constant offset acquisitions were used.

### Data processing

The GPR data were processed with the Reflex-Win 7.5.8 software (Sandmeier, 2014). The processing flow (Figure 3) follows this sequence: (1) Static correction: marks the beginning of the antenna electromagnetic energy from the investigated surface (Olhoeft, 2000); (2) Mean Filter: calculates the average of a trace over a time interval. This filter was used to normalize the high gain present in the first nanoseconds; (3) Background removal: removes background noises (Cassidy,

2009); (4) Gain Function: highlights reflectors using an interactive function that can be linearly and / or exponentially applied at a given depth; (4) Dewow: performs a running average through the data eliminating possible low frequencies.

## RESULTS AND DISCUSSION

The results will be presented as follows: (1) signal analysis to observe the intensity of the energy signal and changes in the amplitudes (2) analysis of reflection patterns, (3) calculation of layer velocities, and (4) layer thickness estimates from GPR antennas and Paired t-test to compare the estimated values versus the actual pavement thickness.

### Signal analysis

In this section, the GPR data amplitude variations from one layer to another within the given frequencies of 270 MHz, 400 MHz, 900 MHz, and 1600 MHz for two pavements. Considering the further correlation of amplitudes coming from different frequencies, a time window of 40 ns was chosen. Only the 270 MHz and 400 MHz frequencies registered 50 ns. However, just the five first layers were identified. The amplitude values were divided by 3200 for a standard plotting with lower values. The limits of the layers were delimited by the amplitude changes and the previously known target depth.

#### Line 1A

Figure 4 displays the processed 1D acquisition of line 1A pavement and the amplitude energy of the envelope trace. The maximum value registered in the envelope trace was 200. Although the Hilbert Transform is a useful tool to identify regions where the amplitude changes (Cunha et al., 2019), in this case, it was not possible to distinguish the boundaries of all layers with all the frequencies used. Only the HRA layer base could be identified by the 270 MHz antenna. Yet, this is not applied to other frequencies. The envelope energy intensity is quite low after its peak in the first 2 ns, recording maximum values of 40% for 270 MHz, 100% for 400 MHz, 30% for 900 MHz, and 50% for 1600 MHz.

Figure 5 shows the 1D acquisitions accomplished for line 1A pavement with processed data and signal envelope (Hilbert Transform). The further descriptions follow from the shallowest to the deepest layer.

Analyzing the envelope energy intensity, it can be inferred that values corresponding to the boundaries of the layers are all close to zero, as occurred in line 1A pavement, which makes it difficult to define the top and bottom of the targets using this processing. The maximum intensities recorded are in the first 2 ns and reach values of 30% for 270 MHz, 100% for 400 MHz, 30% for 900 MHz, and 60% for 1600 MHz.

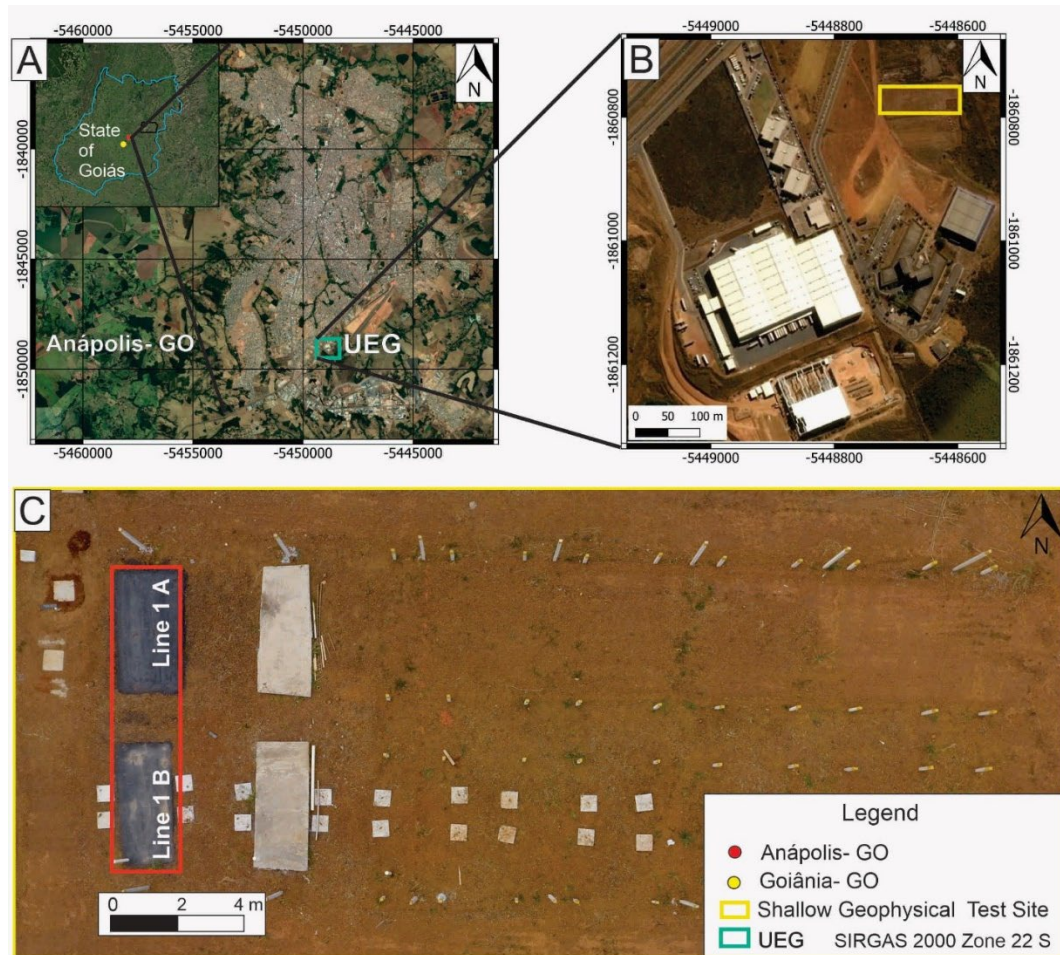


Figure 1: Location map of the SCGRA. (A): State of Goiás-Brazil, (B): the State University of Goiás-Campus Anápolis, and (C): Shallow Geophysical Test Site with the investigated line highlighted in red.

It is notable that after the electromagnetic wave crosses the subbase layer, the amplitudes recorded are close to zero on both pavements (line 1A and line 1B). It is also observed that the amplitude value decreases from the lowest frequency antenna to the highest frequency. This can be explained by the signal energy loss as it reaches greater depths. The attenuation of the electromagnetic wave reduces the amplitude in depth and is proportional to the frequency increase. The attenuation is also influenced by the signal interaction with different material physical properties in the subsurface (Stratton, 1940; Davis & Annan, 1989; Annan, 2003).

### Reflection pattern analysis

The limit on the interface of each layer was highlighted according to the reflection patterns and amplitude responses. All radargrams had the Reflexw plot scale set to 0.3125, given that the GSSI - SIR4000 acquires data with 32-bit binary sampling. This adjusted value establishes a more realistic comparison of the intensity of the amplitudes of the reflecting targets using all antennas. In Figure 6, the radargram sections refer to the profiles acquired in the south-north direction of line 1

which, on the left, it is line 1B pavement and, on the right, line 1A pavement. The profiles were acquired by the 270 MHz, 400 MHz, 900 MHz, and 1600 MHz antennas. In this context, Figure 6A (270 MHz) presents reflectors with bigger amplitudes if compared to Figures 6B (400 MHz), 6C (900 MHz), and 6D (1600 MHz). This is probably due to the amplitude decays according to the antenna frequency. Present in all radargrams between distances 4 and 6 meters from 15 ns, the reflectors show a very low amplitude/marked attenuation. This phenomenon happens because this interval corresponds to a part of unhandled soil that separates the two pavements. Geophysical campaigns previously carried out to acquire the background of the area showed that the GPR signal presents a strong attenuation in the environment, most likely recurring from the presence of clay-sand materials, quite mottled, and with ferricrete (Santos et al., 2019).

Regarding the depth of investigation, it is clear that the frequency of 270 and 400 MHz antennas (Figures 6A and 6B) has a greater range, reaching a time window of 50 ns, while a 900 MHz antenna (Figures 6C) registers approximately 45 ns. The 1600 MHz antenna (Figure 6D) can acquire data up to around 20 ns. After that time, the signal is attenuated, and it is not possible to identify the limits of the other layers.

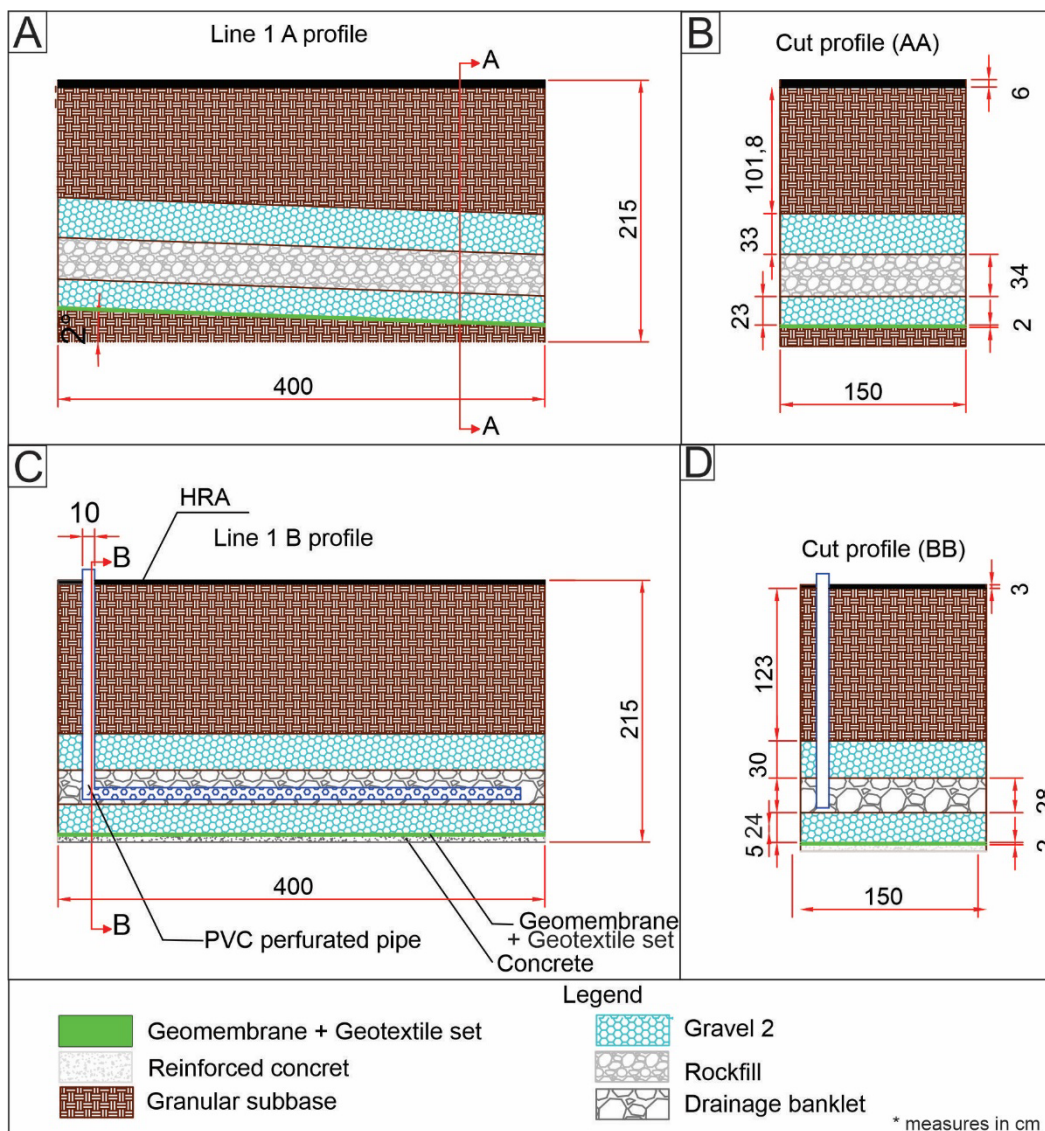


Figure 2: Sketch of the SCGRA containing line 1 (flexible pavement). (A): profile of line 1A; (B): cross-sectional profile of line 1A; (C): profile of line 1B; and (D): cross-sectional profile of line 1B. Note: the thickness of the layers is an average since the thicknesses vary a few centimeters in some sections. Measures are given in centimeters.

Table 1: Acquisition parameters used in this work.

Center frequency (MHz)	Time Range (ns)	Samples	Scan/unit (m)
270	60	2048	300
400		1024	200
900	53.33		300
1600	46.67		

Figure 7 shows the radargram section interpretation. On line 1A pavement, the HRA layer (layer 1) was identified by all antennas. The subbase layers (layer 2), gravel No. 2 (layer 3), rockfill (layer 4), and gravel No. 2 (layer 5) only had their top and bottom limits delimited by the 270 MHz, 400 MHz, and 900 MHz antennas. The 1600 MHz antenna did not identify these layers because of their limited depth of investigation, which can only identify shallower targets.

Also, none of the antennas could identify layers 6 and 7 (geomembrane with geotextile set and reinforced concrete) for several reasons: (1) because of the variety of layers investigated (heterogeneity) that causes signal attenuation with all antennas, (2) the wavelength / resolution of the 270 MHz and 400 MHz antennas (Table 2) that does not allow the identification of the top and bottom of the geomembrane with geotextile set, as this layer is 5 cm thick while the wavelength of these antennas is 9.8

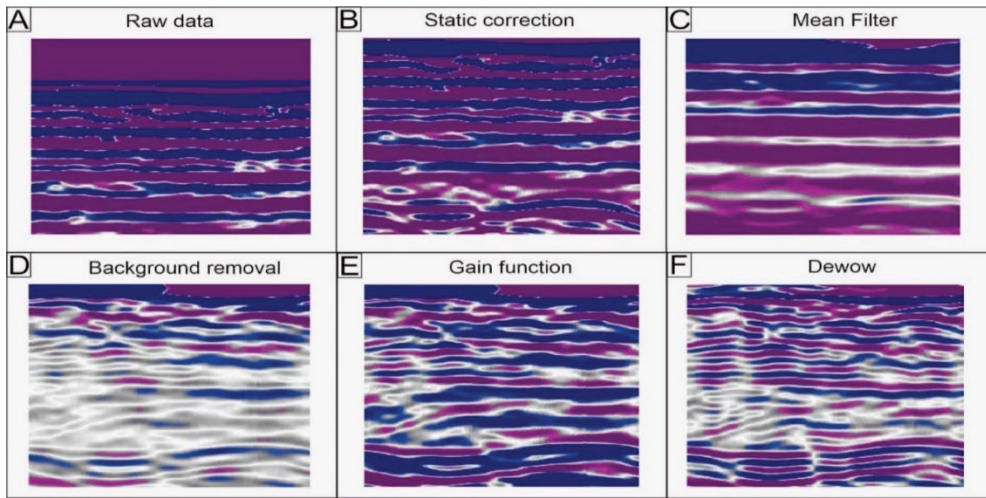


Figure 3: Processing adopted to GPR data with the illustration of the result of each step: (A) raw data, (B) set time zero, (C) mean filter, (D) background removal, (E) data with gain function, and (F) dewow.

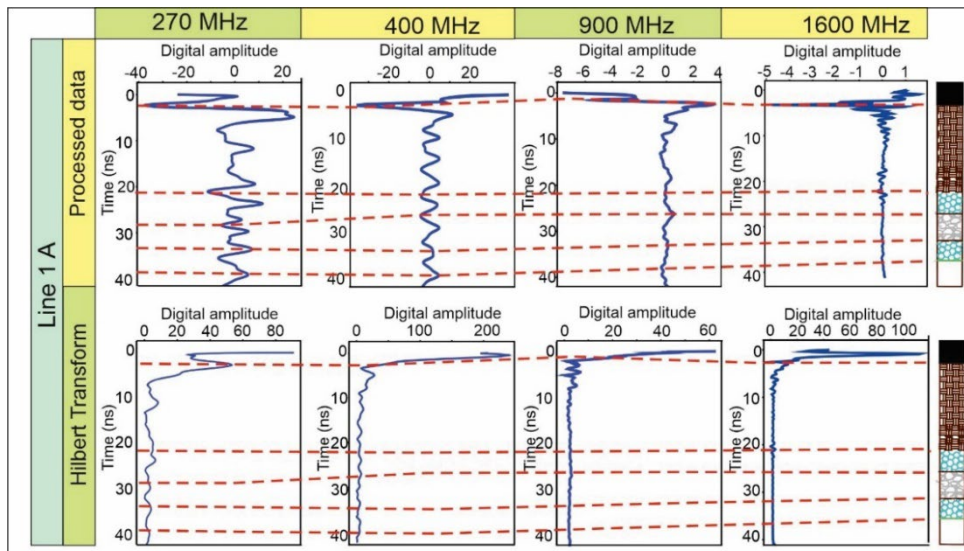


Figure 4: Digital amplitudes of L1A pavement acquired with 270, 400, 900, and 1600 MHz.

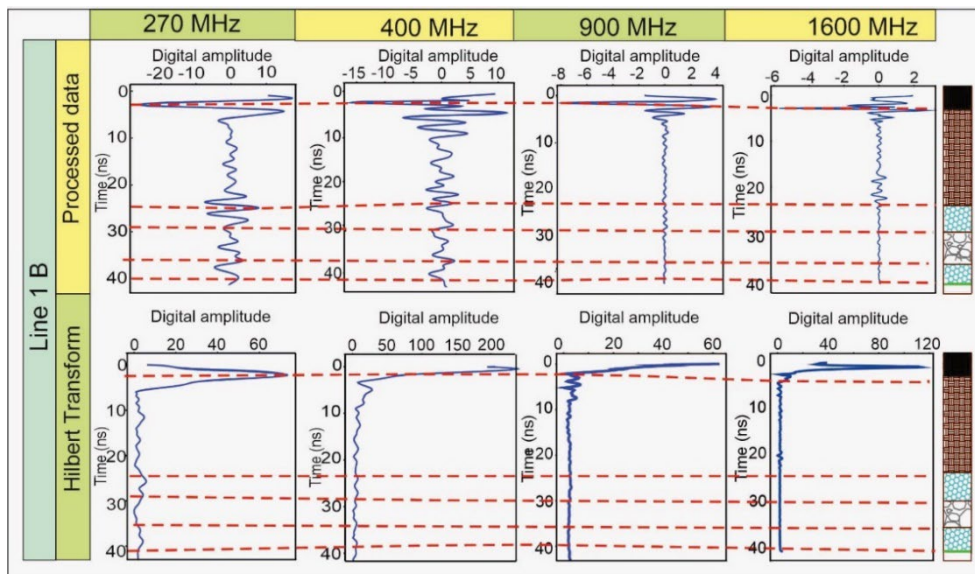


Figure 5: Digital Amplitudes of line 1B pavement acquired by the 270, 400, 900, and 1600 MHz antennas.

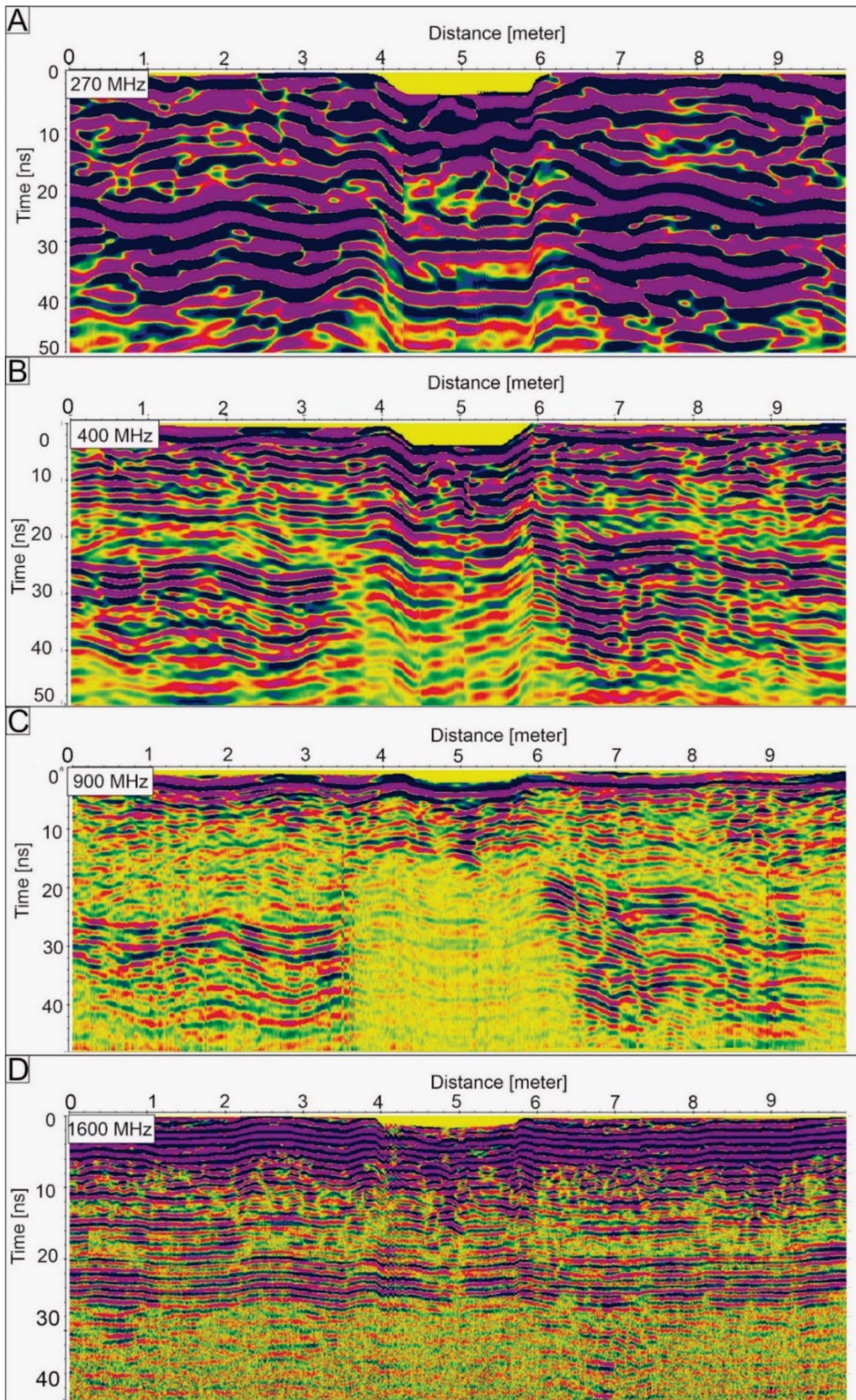


Figure 6: Radargram sections with 4 frequency antennas. (A) 270 MHz antenna, (B) 400 MHz antenna, (C) 900 MHz antenna, and (D) 1600 MHz antenna.

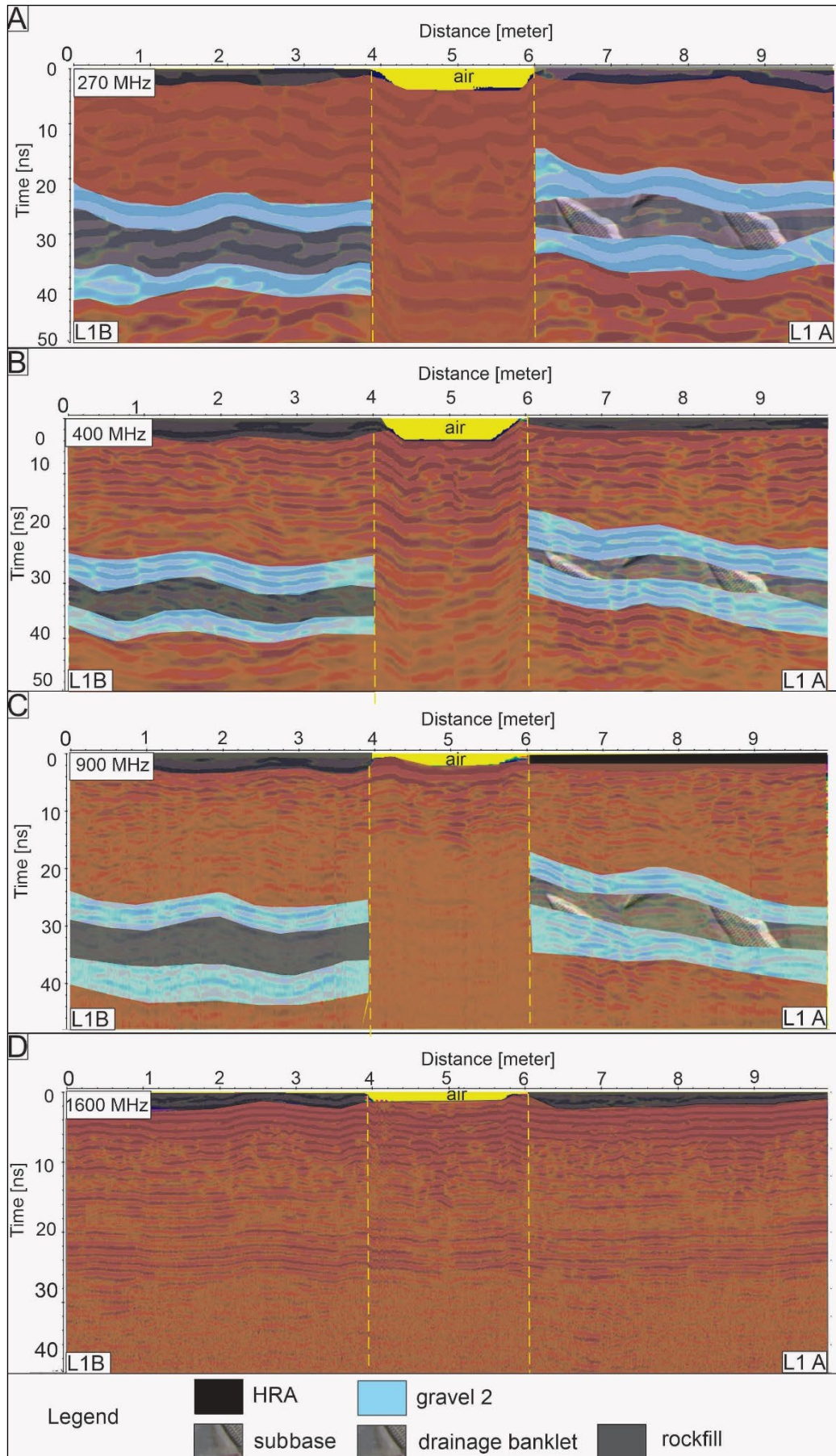


Figure 7: Radargram profiles with their layer interpretation. (A) 270 MHz antenna, (B) 400 MHz antenna, (C) 900 MHz antenna, and (D) 1600 MHz antenna. L1A= line 1 A, L1B= Line 1 B.

and 6 cm respectively. Also, the reinforced concrete that is 2 cm thick would not be bounded by these antennas nor by the 900 MHz antenna. The 1600 MHz antenna would probably be able to identify the top and bottom of these two layers if the medium were more homogeneous.

On line 1B pavement, the boundaries of the HRA layer (layer 1) were identified by all antennas. The top and bottom of the subbase layers (layer 2), gravel No. 2 (layer 3), drainage banklet (layer 4), and gravel No. 2 (layer 5) were delimited by the 270 MHz, 400 MHz, and 900 MHz antennas. The 1600 MHz antenna was unable because of the limited depth of investigation of this frequency.

None of these antennas were able to delimit the geomembrane with geotextile set (layer 6) and the reinforced concrete (layer 7), probably because of the heterogeneity of the medium and the wavelength of the 200 MHz and 400 MHz antennas (Table 2). In contrast, the layer thickness is 2 cm. The 1600 MHz antenna, on the other hand, was unable to identify the top and bottom of layers 2 to 7 because of the limited depth of investigation and heterogeneity of the medium.

### Velocity estimates from GPR

The velocities of the layers were calculated by the average value of each layer thickness. The velocities of the coatings were calculated from the real depth (average) in which the layer base is buried and correlating the reflector to it (equation 1). The velocity (V) depends on the layer thickness ( $2\Delta S$ ) and time (T).

$$v = \frac{2\Delta S}{T} \quad (1)$$

Table 2: Wavelength of each center frequency. Medium velocity: 0.04 m/ns

Center frequency	270 MHz	400 MHz	900 MHz	1600 MHz
Wavelength (cm)	9.8	6.0	2.9	1.6

Tables 3 and 4 present each layer travel time and electromagnetic wave velocity calculated for each antenna.

### Layer thickness estimates and Paired t-test

In order to determine the efficiency of GPR in the identification of asphalt layer thickness, Table 5 shows the average layer thickness estimates from GPR and the average actual layer thickness.

A paired *t*-test ( $\alpha=0.05$ ) was used to compare differences in thickness layers between GPR antenna measurements and average true thickness. No significant differences in the scores for GPR measurements and actual pavement thickness were observed. The 1600

MHz antenna could only identify one layer; with this, it was not possible to apply the *t*-test with this antenna. Table 6 shows the results from the *t*-test analysis for line 1 A and line 1 B.

### CONCLUSIONS

The results of the geophysical campaigns were considered satisfactory, taking into account that they made it possible to identify the top and bottom of the first five layers using the 270 MHz, 400 MHz, and 900 MHz antennas. As expected, the 2 GHz antenna could only delimit the top and bottom of the HRA layers because of the limited depth of investigation. The geomembrane with geotextile set present on the two pavements and the concrete layer (the last layer of the line 1B pavement) were not identified in the radargrams.

The resolution of each antenna is 9.8 cm for 270 MHz; 6.0 cm for 400 MHz; 2.9 for 900 MHz; and 1.6 cm for 1600 MHz.

Concerning layer thickness estimates, the antennas had an efficiency percentage of 83 % (270 MHz and 1600 MHz), 83.29 % (400 MHz), and 84.40 % (900 MHz). The results from the *t*-test showed that the difference between GPR measurements and true thickness was not significant ( $\alpha > 0.05$ ).

Regarding the geomembrane with geotextile set, the main explanation is that this layer is thinner than the wavelengths of the 270 MHz, 400 MHz, and 900 MHz antennas. The 1600 MHz antenna would be the only one capable of delimiting the top and bottom of this layer if it is not located deeper than the antenna range. Another factor that difficult the identification of these layers is the heterogeneity of the environment, which causes the attenuation in the GPR signal. The same pattern of geometry and reflection at the bottom and top of the layers present in all layers of the radargrams corroborates the delimitation of the layers. These standards reaffirm the interpretation of the target limits and emphasize the accuracy of the method in geotechnical studies.

It is clear that the higher the frequency, the shorter the wavelength and, therefore, the better the resolution. However, some information needs to be taken into account before choosing the frequency of the GPR antenna, such as size, geometry, depth in which the target is buried, and heterogeneity of the medium. The sampling interval is also a fundamental parameter for delimiting the borders of a target.

The implementation of the Shallow Geophysical Test Site Applied to Engineering of UEG contributes to the understanding of the GPR method response in asphalt pavements, even though the asphalt pavements studied in this work are not exactly the traditional pavements. Future GPR campaigns on highways are suggested. It is possible to obtain drill hole cores to validate the accuracy and compare geophysical responses in layers with materials other than those presented here.



Table 3: Travel time and velocities of the layers identified by the average real thickness and radargrams obtained by the 270 MHz, 400 MHz, 900 MHz, and 1600 MHz frequency antennas on line 1A. \*\* It was not possible to calculate the layer velocity.

270 MHz		400 MHz		900 MHz		1600 MHz		Layer
t (ns)	v (m/ns)	t (ns)	v (m/ns)	t (ns)	v (m/ns)	t (ns)	v (m/ns)	
1.40	0.085	2	0.06	1.60	0.075	2.09	0.057	C1 (HRA)
19.6	0.010	18	0.11	19.4	0.103	**	**	C2 (subbase)
6		5	0.12	6	0.10	**	**	C3 (gravel No. 2)
6.3	0.104		0.132	5	0.132	**	**	C4 (rockfill)
4.7	0.97	3	0.15	4	0.115	**	**	C5 (gravel No. 2)

Table 4: Travel time and velocities of the layers identified by the average real thickness and radargrams obtained by the 270 MHz, 400 MHz, 900 MHz, and 1600 MHz frequency antennas on line 1B. \*\* It was not possible to calculate the layer.

270 MHz		400 MHz		900 MHz		1600 MHz		Layer
t (ns)	v (m/ns)	t (ns)	v (m/ns)	t (ns)	v (m/ns)	t (ns)	v (m/ns)	
1.2	0.05	1.14	0.05	1.2	0.05	1.07	0.056	C1 (HRA)
23.1	0.106	24.66	0.09	25	0.098	**	**	C2 (subbase)
5.5	0.109	4.2	0.142	3.8	0.157	**	**	C3 (gravel No. 2)
	0.101	4	0.14	8	0.08	**	**	C4 (drainage banklet)
6	0.08	5	0.096	**	**	**	**	C5 (gravel No. 2)

Table 5: Estimated layer thickness obtained by GPR and true thickness (average). Measures are given in centimeters.

Line 1 A					Line 1 B					Layer
270 MHz	400 MHz	900 MHz	1600 MHz	True thickness	270 MHz	400 MHz	900 MHz	1600 MHz	True thickness	
0.08	0.09	0.08	0.08	0.06	0.11	0.14	0.16	0.05	0.03	C1
0.86	0.93	0.95	*	1	0.98	1.02	1.07	*	*	C2
0.3	0.21	0.17	*	0.30	0.25	0.25	0.19	*	*	C3
0.3	0.33	0.36	*	0.33	0.44	0.33	0.35	*	*	C4
0.28	0.32	0.24	*	0.23	0.27	0.26	0.30	*	*	C5

Table 6: Results from the t-test analysis for line 1 A and line 1 B.

Paired t-test	Line 1 A				Line 1 B			
	270 MHz	400 MHz	900 MHz	1600 MHz	270 MHz	400 MHz	900 MHz	1600 MHz
P-value	0.574	0.819	0.467	*	0.8162	0.648	0.834	*
Alpha level	0.05							
Significance	There was not a significant difference in the scores for GPR measurements and actual pavement thickness.							

## ACKNOWLEDGMENTS

The authors would like to thank the Coordenação de Aperfeiçoamento de Pessoal de Nível Superior - CAPES for granting a scholarship for the master's course; to the Goiás State Court of Auditors (TCE) for the support based on agreement No. 001/2018 UEG / TCE-GO; and the Applied Geophysics Laboratory (LGA) of the Institute of Geosciences of the University of Brasília for providing the equipment and support for data processing.

## REFERENCES

- Annan, P.A., 2003, Ground Penetrating Radar Principles, Procedures & Applications: Sensors & Software Inc., Book Manual, 286 pp.
- Aragão, R.C., J.G. Luiz, and P.R.C. Lopes, 2010, Metodologia geofísica aplicada ao estudo arqueológico dos sítios Bittencourt e Jambuaçu, Estado do Pará: Revista Brasileira de Geofísica, **28**, 2, 249–263, doi: [10.1590/S0102-261X2010000200009](https://doi.org/10.1590/S0102-261X2010000200009).
- Borges, W.R., 2007, Caracterização geofísica de alvos rasos com aplicações no Planejamento urbano e Meio ambiente: Estudo sobre o sítio controlado do IAG/USP: PhD Thesis, Instituto de Astronomia, Geofísica e Ciências Atmosféricas, Universidade de São Paulo, SP, Brazil, 265 pp.
- Brasil, D.L., 2013, Investigação Geofísica Forense e Antropológica com o método GPR no cemitério do Tapaná e no cemitério Perdido de Mosqueiro (Belém, Pará): Master Dissertation. Programa de Pós-graduação em Geofísica. Universidade Federal do Pará, Brazil, 94 pp.
- Canata, R.E., F.J. Ferreira, W.R. Borges, and F.A.S. Salvador, 2020, Analysis of 2D and 3D GPR responses in the Federal University of Paraná Forensic Geophysics Controlled Site – A Case Study: Brazilian Journal of Geophysics, **38**, 2, 17 pp, doi: [10.22564/rbgf.v38i2.2045](https://doi.org/10.22564/rbgf.v38i2.2045).
- Cassidy, N.J., 2009, Ground Penetrating Radar Data Processing, Modelling, and Analysis, in JOL, H.M., Ground Penetrating Radar: Theory and Applications: Elsevier Science, chapter 5, p. 141–176, doi: [10.1016/B978-0-444-53348-7.00005-3](https://doi.org/10.1016/B978-0-444-53348-7.00005-3).
- Cavalcanti, M.M., 2017, Estudo da Resposta Geofísica em diferentes cenários de sepultamento: PhD Thesis, Programa de Pós-graduação em Geociências Aplicadas e Geodinâmica, Universidade de Brasília, DF, Brazil, 197 pp.
- Cunha, M.R., W.R. Borges, and L.S. Cunha, 2019, Concrete Pavement Layers Investigation with GPR in the BR-101 Highway: Anuário do Instituto de Geociências, UFRJ, **42**, 1, 308–316, doi: [10.11137/2019\\_1\\_308\\_316](https://doi.org/10.11137/2019_1_308_316).
- Davis, J.L., and P.A. Annan, 1989, Ground-Penetrating Radar for high-resolution Mapping of soil and rock stratigraphy: Geophysical Prospecting, **37**, 531–551, doi: [10.1111/j.1365-2478.1989.tb02221.x](https://doi.org/10.1111/j.1365-2478.1989.tb02221.x).
- Grandjean, G., J.C. Gourry, and A. Bitri, 2000, Evaluation of GPR techniques for civil-engineering applications: study on a test site: Journal of Applied Geophysics, **45**, 141–156, doi: [10.1016/S0926-9851\(00\)00021-5](https://doi.org/10.1016/S0926-9851(00)00021-5).
- Olhoeft, G.R., 2000, Maximizing the information return from Ground Penetrating Radar: Journal of Applied Geophysics, **43**, 175–187, doi: [10.1016/S0926-9851\(99\)00057-9](https://doi.org/10.1016/S0926-9851(99)00057-9).
- Orfanos, C., and G. Apostolopoulos, 2012, Analysis of different geophysical methods in detecting an underground opening at a controlled test site: Journal of the Balkan Geophysical Society, **15**, 1, 7–18.
- Paniagua, J., M. Del Rio, and M. Rufo, 2004, Test site for the analysis of subsoil GPR signal propagation: Tenth International Conference on Ground Penetrating Radar, 21-24 June, 2004, Delft, The Netherlands.
- Porsani, J.L., W.R. Borges, S.I. Rodrigues, and F.Y. Hido, 2006, O Sítio Controlado de Geofísica rasa do IAG/USP: Instalação e Resultados GPR 2D-3D: Revista Brasileira de Geofísica, **24**, 1, 49–61, doi: [10.1590/S0102-261X2006000100004](https://doi.org/10.1590/S0102-261X2006000100004).
- Sandmeier, K.J., 2014, REFLEXW: Version 7.5, Windows 9x/2000/NT, Program for the Processing of Seismic, Acoustic or Electromagnetic Reflection, Refraction, and Transmission Data: Karlsruhe, Germany, 209 pp.
- Santos, A.L.F., T.C. Maia, W.R. Borges, E. Nishi, and E.X. Seimetz, 2019, Implantação do Sítio Controlado de Geofísica Rasa Aplicado a Engenharia da UEG, Campus Henrique Santillo, Anápolis-GO: Revista Mirante, **12**, 95–111.
- Stratton, J.A., 1940, Electromagnetic theory: McGraw-Hill Book Company, Inc., N.Y. and London, 648 pp.

**Moreira, J.S.:** methodology, data acquisition, processing, interpretation, writing; **Lopes Paula, M.C.:** methodology, data acquisition, processing, writing; **Borges, W.R.:** work supervisor, methodology, corrections; **Santos, A.L.F.:** co-supervisor, equipment loan, data acquisition; **Seimetz, E.X.:** methodology, processing help.

Received on December 29, 2021 / Accepted on April 15, 2022